Free-Electron Laser Design for Four-Wave Mixing Experiments with Soft-X-Ray Pulses

G. Marcus,[1,2] G. Penn,[2] and A. A. Zholents[3]

[1] *Lawrence Berkeley National Laboratory, Berkeley, California 94720, USA*
[2] *SLAC National Accelerator Laboratory, Menlo Park, California 94025, USA*
[3] *Argonne National Laboratory, Argonne, Illinois 60439, USA*

10 July 2014

Published in Physical Review Letters **113**, 024801 (2014)

This work was supported by the Director, Office of Science, Office of Basic Energy Sciences, of the U.S. Department of Energy under Contracts No. DE-AC02-05CH11231, No. DE-AC02-06CH11357, and No. DE-AC02-76SF00515.

Free-Electron Laser Design for Four-Wave Mixing Experiments with Soft-X-Ray Pulses

G. Marcus,[1,2] G. Penn,[1] and A. A. Zholents[3]

[1]*Lawrence Berkeley National Laboratory, Berkeley, California 94720, USA*
[2]*SLAC National Accelerator Laboratory, Menlo Park, California 94025, USA*
[3]*Argonne National Laboratory, Argonne, Illinois 60439, USA*

(Dated: 10 July 2014)

We present the design of a single-pass free-electron laser amplifier suitable for enabling four-wave mixing x-ray spectroscopic investigations. The production of longitudinally coherent, single-spike pulses of light from a single electron beam in this scenario relies on a process of selective amplification where a strong undulator taper compensates for a large energy chirp only for a short region of the electron beam. This proposed scheme offers improved flexibility of operation and allows for independent control of the color, timing and angle of incidence of the individual pulses of light at an end user station. Detailed numerical simulations are used to illustrate the more impressive characteristics of this scheme.

PACS numbers: 41.60.Cr, 41.50.+h,42.55.Vc

The unequivocal success of existing x-ray free-electron lasers (XFELs) such as FLASH [1], LCLS [2], SACLA [3], and Fermi@elettra [4] has been followed by further development and demonstration of expanded facility capabilities such as implementation of hard x-ray self seeding at LCLS [5], obtaining two-pulse, two-color jitter free x rays at LCLS [6, 7] and Fermi@elettra [8, 9], and improvements in the temporal coherence of SASE at LCLS [10]. The high intensity electromagnetic fields produced by XFELs could also allow us to extend a vast arsenal of nonlinear optics techniques to x rays [11–15]. Using x rays to perform a broad variety of four-wave mixing (FWM) spectroscopies (see, e.g., [16–21]) is of particular importance. Major breakthroughs are expected from the addition of atomic element selectivity provided by x rays when a high frequency field ω_1 resonantly excites a higher-lying energy state e, as depicted in Fig. 1(a), while a second high frequency field ω_2 stimulates transition to a low-lying state f followed by excitation of the wave-function packet shared by valence electrons. Therefore, an energy balance $\hbar\omega_{\rm ex} = \hbar\omega_1 - \hbar\omega_2$ comparable to the energy band of valence electrons $\sim$ 1–10 eV is desirable for most experiments. Here $\hbar$ is Planck's constant. This wave-function packet is subsequently probed after some time delay τ by a third high frequency field ω_3 tuned at the core resonance either of the same atom (e.g., $\omega_3 = \omega_1$) or a different atom of a molecule, and a FWM signal with the frequency ω_4 is produced. An efficient signal generation occurs along a so-called phase-matched direction $\vec{k}_4 = \vec{k}_1 - \vec{k}_2 + \vec{k}_3$, where constructive interference (in phase addition of scattered amplitudes) of all fields takes place [see Fig. 1(b)]. Here, $\vec{k}_i$ (i=1–4) is the wave vector of the corresponding field. Remarkably, $\vec{k}_4$ can often be arranged to have a different direction from any of the incoming fields such as to improve the signal-to-noise ratio of a relatively weak FWM signal.

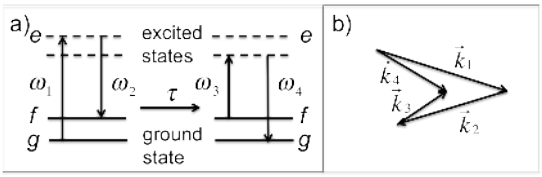

FIG. 1: Schematic representation of FWM spectroscopy. (a) The wave-function packet of valence electrons is excited at one atom and probed with a time delay at another atom. (b) The phase matching condition defines the direction at which the signal is detected.

The production of x-ray pulses needed for the FWM experiments, however, is far from a trivial matter. Temporal coherence, exquisite synchronization, and high intensities are essential requirements. In addition, x rays with a bandwidth comparable to the energy band of valence electrons is crucial. The latter may be attained using either sub-femtosecond pulses or pulses with large frequency chirps.

To the best of our knowledge, only two XFEL proposals published to date meet, in principle, the above requirements [22, 23]. In [22], current enhanced SASE [24] is combined with echo-enabled harmonic generation [25] to produce two temporally coherent soft-x-ray pulses with a variable time delay, a wide bandwidth (up to $\sim$10 eV), and frequencies that can be independently tuned over a broad range. This proposal was extended in [23] by adding the third soft-x-ray pulse in a fashion similar to [22] and by explicitly showing how all three pulses can be recombined on a sample with adjustable angles of incidence and variable time delays. Alternatively, the wide bandwidth enables any pulse to be split into two (or more) pulses by employing diffraction gratings. However, inherent to the technique employed in [22, 23] is coherent radiation from weakly prebunched electrons that produce relatively low field intensities by FEL standards.

It should also be emphasized that intrabeam Coulomb scattering of electrons (not analyzed in [22, 23]) could potentially limit attainable bunching for the production of high frequency radiation as discussed in [26].

Here we present a different approach, where two self-amplified spontaneous emission (SASE) XFELs sharing the same electron bunch produce two wide bandwidth x-ray pulses in the soft-x-ray spectral range. Subsequently, one of these pulses is directed onto a diffraction grating to obtain two pulses with a small frequency separation. We demonstrate that this approach has all the benefits of the technique discussed in [22, 23], but is not sensitive to intrabeam Coulomb scattering and has the advantage of higher x-ray pulse intensity.

The method presented here relies on the interplay between a laser modulated electron beam possessing a large energy chirp, given by $\alpha_c = d\gamma/ds$ along only a short section of the bunch, and a strongly tapered undulator. Here, γ is the electron energy (normalized to the rest energy) and s is the electron coordinate with respect to the center of the bunch. As shown in [27–31], the impact of the linear energy chirp on the FEL gain can be balanced by a corresponding undulator taper:

$$\frac{dK}{dz} = \frac{1}{K_0}\left(1+\frac{K_0^2}{2}\right)^2 \frac{\alpha_c}{\gamma_0^3}\,, \qquad (1)$$

where z is the coordinate along the undulator, $K_0 = eB_0\lambda_u/(2\pi mc)$ is the undulator parameter, B_0 is the undulator peak magnetic field in the middle of the undulator, λ_u is the undulator period, e and m are the electron charge and mass, c is the speed of light, and γ_0 is the nominal electron energy. This taper simultaneously suppresses gain in the electron bunch regions without a corresponding energy chirp. The length of the energy chirped region can be made equal to (or shorter than) the temporal coherence length, $\sim 4L_g\lambda_x/\lambda_u$ for SASE near saturation [32, 33], to obtain a coherent x-ray pulse for FWM experiments. Here L_g is the FEL gain length and λ_x is the wavelength of the x-ray radiation. In addition, this process can be repeated at multiple longitudinal locations to produce several independently tuned FEL pulses from a single electron beam.

A schematic of the method is shown in Fig. 2. A single-cycle carrier-envelope-phase-stable mid-IR laser is split into two pulses, the first of which is injected into a one-period wiggler, W_1. The longitudinal electric field of the seed laser is imprinted as an energy modulation on the electron beam, which takes the following idealized form:

$$\Delta\gamma(s) = \Delta\gamma_0 \sin\left[k_L(s-s_1)\right] e^{-(s-s_1)^2/2\sigma_L^2}\,, \qquad (2)$$

where $k_L = 2\pi/\lambda_L$ is the laser wave number, σ_L is the rms width of the Gaussian envelope for the laser electric field, s_1 is the center of the 1st modulation region, and $\Delta\gamma_0$ is the energy modulation amplitude calculated according to [34, 35]. We take the beam parameters to be 2.4 GeV energy, 500 A peak current, 200 keV energy spread, and 0.6 μm emittance [36]. For this beam, it would take a pulse energy of ~ 200 μJ for a single-cycle seed laser at $\lambda_L = 5$ μm to obtain $\Delta\gamma_0 = 10$. Figure 3 shows the resulting electron energy modulation if the phase of the laser were selected such that the peak of the laser intensity is coincident with the electric field zero crossing. Here, the energy chirp is roughly linear. It will be shown below that choosing this set of parameters promotes a condition when the FEL lasing in the *main* region (see Fig. 3) significantly dominates lasing in the *side* regions. However, if a single-cycle laser pulse is not available, more elaborate techniques using longer pulses to achieve a similar result can also be employed (see, e.g., [35, 37]).

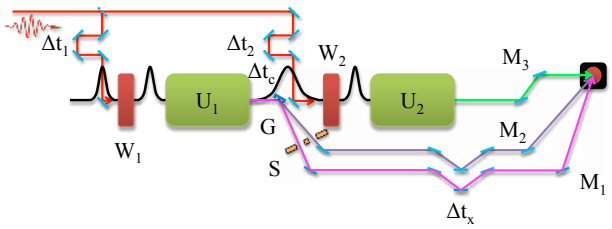

FIG. 2: Schematic of a soft-x-ray FEL facility: W_1 and W_2 are modulators, U_1 and U_2 are undulators, Δt_1 and Δt_2 are seed laser delay stages, Δt_c is the electron beam chicane delay, Δt_x is the x-ray delay line, G is the grating, S is the slit, and $M_{1,2,3}$ are adjustable x-ray mirrors.

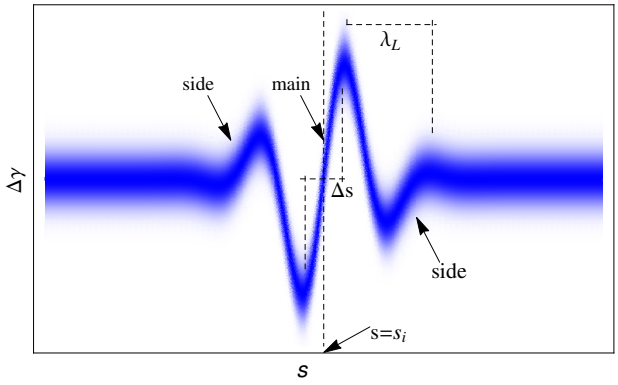

FIG. 3: A density plot for a fragment of the electron bunch longitudinal phase space centered around $s = s_i$, showing energy deviation for a modulated electron bunch. As discussed in the text, an undulator taper is selected to fully compensate the energy chirp in the *main* region with the length Δs while it only partially compensates energy chirps in the *side* regions.

The electron bunch next encounters a trimming chicane before proceeding into the first undulator, U_1, that allows for slight adjustments to the energy chirp using

the chicane's time-of-flight parameters $R_{56}^{(i)}$:

$$\alpha_c \simeq k_L \Delta\gamma_0 \left(1 - \frac{\Delta\gamma_0}{\gamma_0} k_L R_{56}^{(i)}\right) . \quad (3)$$

In addition, this process stretches the *main* region from $\Delta s \simeq \lambda_L/2$ to $\Delta s^{(i)} \simeq \lambda_L/2 + 2R_{56}^{(i)}\Delta\gamma_0/\gamma_0$ and assists in obtaining a condition when only a single temporally coherent pulse reaches full saturation in the amplification process. The choice of $\lambda_L = 5$ μm for this study was informed first by estimating the FEL performance using various fitting formulas [33, 38, 39], consulting Eqs. (2), (3), and ultimately through `GENESIS` [40] simulations such that FEL lasing was supported for x-ray photon energies from 250 to 1000 eV. The low end of this energy range is delimited by the increasing coherence length, while the high end is constrained by the beam quality and resonance condition.

The electron bunch then passes through an undulator U_1 composed of several 3 m long sections interspersed with strong focusing quadrupoles. These sections are tapered in discrete steps approximating Eq. (1) for $\alpha_c \approx 13$ μm^{-1}. In this way, a single x-ray pulse is produced in the linearly chirped region of the bunch which amplifies to saturation at the end of the 10th undulator section. Remarkably, the rest of the electron bunch barely radiates and the beam quality is not impacted. Therefore, it is possible to repeat the selective amplification process at a different location along the electron bunch. In the specific example presented here for illustrative purposes, the undulator parameter of U_1 is tuned to produce photons with energy $\sim$ 1000 eV, i.e., at the high end of a spectral tuning range, which is typically the most difficult for FELs. We note that due to the large energy chirp in the electron bunch the x-ray pulse also has a large energy chirp of $\alpha_x \simeq 5$ eV/μm with energy variation $\sim$ 7 eV shown in Fig. 4.

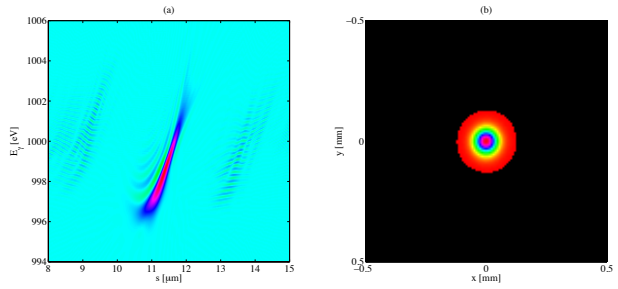

FIG. 4: (a) Normalized Wigner transform of the on-axis far field FEL radiation. (b) Projected transverse profile of the near field intensity.

After U_1 the electron bunch proceeds into a small chicane used to accommodate a diffraction grating (G) and mirror to inject a second laser pulse in W_2. The grating angular dispersion maps frequency to transverse position, which allows downstream slits and mirrors to assist in the selection of two x-ray pulses with nearby frequencies ω_1 and ω_2. Further downstream, two x-ray delay stages (Δt_x) allow adjustment of the arrival times on the sample for these pulses. The chicane also serves to destroy any enhanced electron bunching [41] to avoid FEL interaction in the downstream undulator U_2.

The second half of the scheme after this point is identical to the first. The electron bunch is energy modulated in a second wiggler (W_2) at a longitudinal position s_2 that is not coincident with s_1. The distance between the energy modulations is controlled by two laser pulse delay stages Δt_1 and Δt_2 and the electron bunch delay Δt_c from the previous chicane, establishing broad timing flexibility. The bunch then proceeds into the undulator U_2 tuned to produce a third x-ray pulse with frequency ω_3. The flexibility and high precision control over the timing between all three x-ray pulses is a key feature of this design, allowing the order and arrival times of the three x-ray pulses at the sample to vary all the way down to zero timing differential.

The x-ray pulses produced in this scheme are spatially separated. Therefore, the angle of incidence at the sample for each of the three pulses can be controlled with x-ray optics (e.g., M_1, M_2, M_3). This flexibility is crucial for advanced multidimensional spectroscopic experiments. A specific design of a system implementing this flexibility is out of the scope of this Letter and will be addressed in a forthcoming paper.

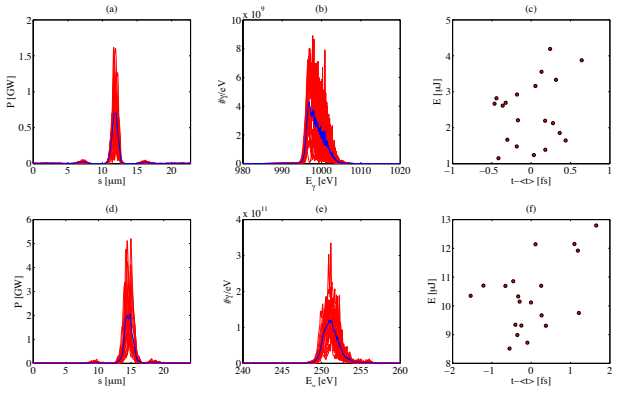

FIG. 5: X-ray pulse characteristics for 1000 eV (a),(b),(c) and 250 eV (d),(e),(f). Peak power (a),(d) and spectrum (b),(e) for single simulation runs (red, thin curves) and averaged over twenty simulation runs (blue, thick curves). Scatter plots (c),(f) of the x-ray pulse energy and the arrival time deviations from the average time.

Numerical simulations using the FEL code `GENESIS` were utilized to evaluate the performance of the system under ideal conditions. The results of twenty independent SASE simulations where the undulator is tuned to produce 1000 eV photons are shown in the temporal and spectral domains in Figs. 5(a) and 5(b), respectively. The

temporal profile is dominated by one pulse containing ~ 4 times more photons than the number of photons outside of it (assuming a 300 fs long pulse). Two *side* regions in Fig. 3 also see a small FEL gain and produce two weak pulses seen in Figs. 5(a). Because of SASE, there is jitter in the pulse energy and in the pulse arrival time. This is clearly seen in Fig. 5(c), which is a scatter plot showing the pulse energy and arrival time deviations for the twenty independent SASE runs. The standard deviation for the temporal jitter distribution is only ~ 0.3 fs and for the energy jitter is ~ 0.9 μJ. The arrival time of the pulses is also influenced by the electron beam energy jitter. Achieving 0.3 fs timing jitter requires relative energy jitter to be less than 10^{-4}. This requirement will also keep the photon energy jitter below 0.2 eV, which is much less than the bandwidth. Other slow timing drifts will be controlled by a feedback system. The average x-ray pulse energy is ~ 2.4 μJ, corresponding to 1.5×10^{10} photons per pulse. The dominant transverse mode for this radiation has a 11.3 m Rayleigh range and contains 90.1±5.7% of the pulse energy on average for the twenty simulations. A typical transverse profile is shown in Fig. 4(b). The temporal, spectral, and energy jitter characteristics when the undulators are tuned to produce 250 eV photons are illustrated in Figs. 5(d)–5(f). An example FWM experiment could split the radiation at 1000 eV from the first stage into two pulses centered about 997 and 1001 eV, and use the radiation at 250 eV from the second stage as is for the third pulse.

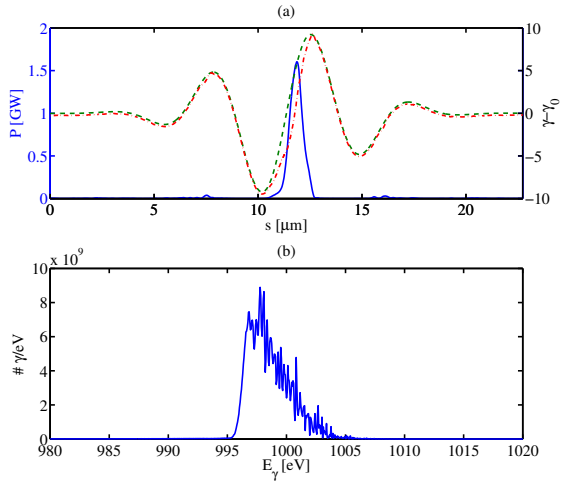

FIG. 6: (a) Power (blue), and initial (green, dashed) and final (red, dotted-dashed) deviations in the slice energy as a function of the longitudinal coordinate along the pulse, s. (b) Spectrum.

It is useful, at this point, to analyze the individual photon beam characteristics of a typical pulse resulting from the chirp and taper combination. Figure 6(a) shows the longitudinal profile of the light (blue) resulting from the selective amplification process in relation to the initial (green) and final (red) e-beam slice energies. The x-ray pulse is well localized within the gain compensation region and has a peak power of ~ 1.6 GW and FWHM temporal duration of $\Delta t \sim 2.4$ fs. The number of photons contained within this region is greater than 2×10^{10}. Figure 6(b) shows the spectral content of this pulse where the FWHM bandwidth, $\Delta E_\gamma \sim 4.4$ eV, is much greater than the nominal SASE bandwidth of an unmodulated electron bunch in an untapered undulator. This is a result of the very large e-beam energy chirp which produces a chirped FEL pulse. The lowest photon energies occur in the head of the pulse and had to be produced in the final undulators, both because of the taper and because the FEL gain curve exhibits a cutoff at low photon energies. The time bandwidth product, about 5 times the Fourier transform limit in this case, is a direct consequence of the chirp. This pulse can potentially be further compressed using high efficiency x-ray gratings with asymmetric cut multilayers [42] to $\Delta t \sim 560$ attoseconds.

In summary, we have presented a design for a FEL beam line suitable for FWM spectroscopy within a large spectral range (250–1000 eV). The production of radiation in this scenario relies on a selective amplification process that employs an energy-chirped electron beam and a tapered undulator. Here, 2 out of 3 x-ray pulses needed for FWM have carrier frequencies separated by only a few eV. Although this is not a large number, in many cases this is all that is needed to match the width of the energy band of valence electrons. A third modulator and radiator stage can be included if a large frequency separation between all three x-ray pulses is important. Finally, although the Letter was focused on implementation of FWM spectroscopy, the same facility can be used for a broader variety of experiments and experimental techniques including transient grating spectroscopic methods [43]. The advanced capabilities offered by all these experimental techniques are sure to revolutionize x-ray science.

The authors would like to thank Y. Ding and Z. Huang for many helpful and insightful discussions. This work was supported by the Director, Office of Science, Office of Basic Energy Sciences, of the U.S. Department of Energy under Contracts No. DE-AC02-05CH11231, No. DE-AC02-06CH11357, and No. DE-AC02-76SF00515.

[1] W. Ackermann, G. Asova, V. Ayvazyan, A. Azima, N. Baboi, J. Bahr, V. Balandin, B. Beutner, A. Brandt, A. Bolzmann, et al., Nature Photonics **1**, 336 (2007).
[2] P. Emma, R. Akre, J. Arthur, R. Bionta, C. Bostedt, J. Bozek, A. Brachmann, P. Bucksbaum, R. Coffee, F. J. Decker, et al., Nature Photonics **4**, 641 (2010).
[3] T. Ishikawa, H. Aoyagi, T. Asaka, Y. Asano, N. Azumi, T. Bizen, H. Ego, K. Fukami, T. Fukui, Y. Furukawa,

et al., Nature Photonics **6**, 540 (2012).
[4] E. Allaria, R. Appio, L. Badano, W. A. Barletta, S. Bassanese, S. G. Biedron, A. Borga, E. Busetto, D. Castronovo, P. Cinquegrana, et al., Nature Photonics **6**, 699 (2012).
[5] J. Amann, W. Berg, V. Blank, F.-J. Decker, Y. Ding, P. Emma, Y. Feng, J. Frisch, D. Fritz, J. Hastings, et al., Nature Photonics **6**, 693 (2012).
[6] A. A. Lutman, R. Coffee, Y. Ding, Z. Huang, J. Krzywinski, T. Maxwell, M. Messerschmidt, and H.-D. Nuhn, Phys. Rev. Lett. **110**, 134801 (2013).
[7] A. Marinelli, A. A. Lutman, J. Wu, Y. Ding, J. Krzywinski, H.-D. Nuhn, Y. Feng, R. N. Coffee, and C. Pellegrini, Phys. Rev. Lett. **111**, 134801 (2013).
[8] G. De Ninno, B. Mahieu, E. Allaria, L. Giannessi, and S. Spampinati, Phys. Rev. Lett. **110**, 064801 (2013).
[9] E. Allaria, F. Bencivenga, R. Borghes, F. Capotondi, D. Castronovo, P. Charalambous, P. Cinquegrana, M. Danailov, G. De Ninno, A. Demidovich, et al., Nat. Commun. **4:2476**, 1 (2013).
[10] J. Wu, C. Pellegrini, A. Marinelli, H.-D. Nuhn, F.-J. Decker, H. Loos, A. Lutman, D. Ratner, Y. Feng, J. Kryzwinski, et al., Proceedings of IPAC2013, Shanghai, China, 12-17 May, 2013 (2013).
[11] S. Tanaka and S. Mukamel, Journal of Chemical Physics **116**, 1877 (2002).
[12] S. Tanaka and S. Mukamel, Phys. Rev. Lett. **89**, 043001 (2002).
[13] B. Patterson, Report SLAC-TN-10-026, SLAC (2010).
[14] J. D. Biggs, Y. Zhang, D. Healion, and S. Mukamel, Journal of Chemical Physics **136**, 174117 (2012).
[15] L. Misoguti, I. P. Christov, S. Backus, M. M. Murnane, and H. C. Kapteyn, Phys. Rev. A **72**, 063803 (2005).
[16] D. Avisar and D. J. Tannor, Phys. Rev. Lett **106**, 170405 (2011).
[17] S. Mukamel, D. Healion, Y. Zhang, and J. D. Biggs, Annual Review of Physical Chemistry **64**, 101 (2013).
[18] G. Dadusc, J. P. Ogilvie, P. Schulenbert, U. Marvet, and R. J. D. Miller, Proc. National. Acad. Sci. **98**, 6110 (2001).
[19] M. A. Foster, A. C. Turner, J. E. Sharping, B. S. Schmidt, M. Lipson, and A. L. Gaeta, Nature **441**, 960 (2006).
[20] X. Li, P. L. Voss, J. E. Sharping, and P. Kumar, Phys. Rev. Lett **94**, 053601 (2005).
[21] H. Kim, G. W. Bryant, and S. J. Stranick, Opt. Express **20**, 6042 (2012).
[22] A. Zholents and G. Penn, Nuclear Instruments and Methods A **612**, 254 (2010).
[23] F. Bencivenga, S. Baroni, C. Carbone, M. Chergui, M. B. Danailov, G. D. Ninno, M. Kiskinova, L. Raimondi, C. Svetina, and C. Masciovecchio, New J. of Phys. **15**, 123023 (2013).
[24] A. A. Zholents, Phys. Rev. ST Accel. Beams **8**, 040701 (2005).
[25] G. Stupakov, Phys. Rev. Lett. **102**, 074801 (2009).
[26] G. Stupakov, Proceedings of the 33rd International Free Electron Laser Conference, Shanghai, China (2011).
[27] E. L. Saldin, E. A. Schneidmiller, and M. V. Yurkov, Phys. Rev. ST Accel. Beams **9**, 050702 (2006).
[28] Z. Huang, Y. Ding, and J. Wu, Proceedings of the 32nd International Free Electron Laser Conference, Malmö, Sweden (2010).
[29] L. Giannessi, A. Bacci, M. Bellaveglia, F. Briquez, M. Castellano, E. Chiadroni, A. Cianchi, F. Ciocci, M. E. Couprie, L. Cultrera, et al., Phys. Rev. Lett. **106**, 144801 (2011).
[30] G. Marcus, M. Artioli, A. Bacci, M. Bellaveglia, E. Chiadroni, A. Cianchi, F. Ciocci, M. D. Franco, G. D. Pirro, M. Ferrario, et al., Applied Physics Letters **101**, 134102 (pages 4) (2012).
[31] W. Fawley, Nuclear Instruments and Methods A **593**, 111 (2008), fEL Fronties 2007: Proceedings of the International Workshop on Frontiers in FEL Physics and Related Topics.
[32] S. Krinsky, AIP Conference Proceedings **648**, 23 (2002).
[33] R. Bonifacio, L. De Salvo, P. Pierini, N. Piovella, and C. Pellegrini, Phys. Rev. Lett. **73**, 70 (1994).
[34] A. Zholents and K. Holldack, Proceedings of the 28th International Free Electron Laser Conference, Berlin, Germany (2006).
[35] A. A. Zholents and G. Penn, Phys. Rev. ST Accel. Beams **8**, 050704 (2005).
[36] G. Penn, P. Emma, G. Marcus, J. Qiang, and M. Reinsch, Proceedings of the 35th International Free Electron Laser Conference, New York, USA (2013).
[37] Y. Ding, Z. Huang, D. Ratner, P. Bucksbaum, and H. Merdji, Phys. Rev. ST Accel. Beams **12**, 060703 (2009).
[38] M. Xie, Nuclear Instruments and Methods A **445**, 59 (2000).
[39] G. Marcus, E. Hemsing, and J. Rosenzweig, Phys. Rev. ST Accel. Beams **14**, 080702 (2011).
[40] S. Reiche, Nuclear Instruments and Methods A **429**, 243 (1999).
[41] E. A. Schneidmiller and M. V. Yurkov, Phys. Rev. ST Accel. Beams **16**, 110702 (2013).
[42] S. Bajt, H. N. Chapman, A. Aquila, and E. Gullikson, J. Opt. Soc. Am. A **29**, 216 (2012).
[43] K. A. Nelson, R. J. D. Miller, D. R. Lutz, and M. D. Fayer, J. Appl. Phys **53**, 1144 (1982).